A new constitutive model for permanent deformation of blood clots with application to simulation of aspiration thrombectomy

Behrooz Fereidoonnezhad[1], Patrick McGarry[1],*

School of Engineering, National University of Ireland Galway, Galway, Ireland

Abstract

Direct aspiration with large bore catheter as the first line option in treatment of acute Ischemic stroke (AIS) is a fast and effective technique with promising outcomes. In silico models are widely used for design and preclinical assessment of new developed devices and therapeutic methods. Accurate modelling of the mechanical behaviour of blood clot is a key factor in the design and simulation of aspiration devices. In this study we develop a new constitutive model which incorporates the unrecoverable plastic deformation of clots. The model is developed based on the deformation-induced microstructural changes in fibrin network, including the formation and dissociation of the cross-links between fibrin fibres. The model is calibrated using previously reported experimentally measured permanent clot deformation following uniaxial stretching. The calibrated plasticity model is then used to simulate aspiration thrombectomy. Results reveal that inclusion of permanent plastic deformation results in ~15 % increase in clot aspiration length at an applied aspiration pressure of 200 mmHg. The constitutive law developed in this study provides a basis for improved design and evaluation of novel aspiration catheters leading to increased first-pass revascularization rate.

Keywords: *Acute ischemic stroke, Aspiration thrombectomy, Blood clot, Computational modelling, permanent deformation*

[1] Corresponding author: Patrick.mcgarry@nuigalway.ie

1. Introduction

Acute Ischemic Stroke (AIS), mainly caused by intracranial large vessel occlusions, is the second leading cause of death worldwide ("WHO global health estimate," 2020). Mechanical Thrombectomy (MT) is an established non-invasive treatment of large vessel occlusion. Despite significant improvement of MT method in recent years, the proportion of patients experiencing successful procedural revascularization (TICI >=2b) ranged from 76% (Maus et al., 2018) to 85.4% (Chueh et al., 2011) after all procedures. Although complete revascularization (TICI =3) is achieved in less than 61% of cases (Yoo and Andersson, 2017), and it often takes multiple attempts to remove the complete thrombus. First pass revascularisation is associated with better clinical outcome. Revascularization in multiple passes leads to complications such as increased risk of distal embolization due to the clot fragmentation (Fereidoonnezhad et al., 2020a; Gralla et al., 2006; Kaesmacher et al., 2017; Po Sit, 2009). Moreover, a recent study shows that successful first pass recanalization in MT in US and EU reduces hospitalization and care costs in first year after stroke (Zaidat et al., 2020). In order to maximize the number of patients with first-pass revascularization, new AIS therapies have been developed. One such therapy that has attracted attentions in the recent years is A Direct Aspiration first Pass Technique (ADAPT) in which a large bore catheter is used for clot aspiration. Clinical studies demonstrate that ADAPT is fast and effective for vessel recanalization as the first line option, results in quick and successful revascularization in more than 50% of patients (Kowoll et al., 2016).

Development of improved design and simulation of aspiration thrombectomy devices is highly dependent on accurate modelling of the mechanical behaviour of blood clots. The authors recently developed hyperelastic constitutive model which have been shown to replicate the isochoric and volumetric deformation of thrombi during compression and tension tests (Fereidoonnezhad et al., 2021, 2020b). The main objective of the current paper is to incorporate permanent (unrecoverable) deformation, as reported in recent experimental investigations (Sugerman et al., 2020). The current study develops a physically based thermodynamically consistent model based on inelastic deformation of the fibrin network, including the stretch-dependent formation and dissociation of cross-links between fibrin fibers. the model is developed withing the framework of finite deformation plasticity theory employing a multiplicative decomposition of the deformation gradient into an elastic and plastic part. The framework is calibrated using reported experimental data (Sugerman et al., 2020) and is used to simulate the aspiration of a clot into an aspiration catheter. Results reveal that permanent deformation leads to a significant (15 %) increase in clot aspiration length in comparison to predictions that assume a hyperplastic clot without inclusion of plasticity mechanisms.

2. Continuum modelling

Blood clots exhibit complex mechanical behaviour (Fereidoonnezhad et al., 2021; Johnson et al., 2020, 2019). In our previous studies (Fereidoonnezhad et al., 2021, 2020b), we have characterised the nonlinear hyperelastic behaviour of clots, including elastic deformation and reorientation of the fibrin network. In the current study we extend our previous hyperelastic modelling framework to incorporate permanent inelastic deformation of clots based on formation and dissociation of the cross-links between fibrin fibres.

2.1 *Kinematics*

In this constitutive framework a multiplicative decomposition of deformation gradient tensor $\mathbf{F}$ is employed, such that:

$$\mathbf{F} = \mathbf{F}_e\mathbf{F}_p \tag{1}$$

The spatial velocity gradient $\boldsymbol{l}$ is then given as:

$$\boldsymbol{l} = \dot{\mathbf{F}}\mathbf{F}^{-1} = \dot{\mathbf{F}}_e\mathbf{F}_e^{-1} + \mathbf{F}_e\left(\dot{\mathbf{F}}_p\mathbf{F}_p^{-1}\right)\mathbf{F}_e^{-1} \tag{2}$$

A pull-back of the spatial velocity gradient to the intermediate configuration leads to

$$\mathbf{L} = \mathbf{F}_e^{-1}\boldsymbol{l}\,\mathbf{F}_e = \mathbf{L}_e + \mathbf{L}_p, \qquad \mathbf{L}_e = \mathbf{F}_e^{-1}\dot{\mathbf{F}}_e, \qquad \mathbf{L}_p = \dot{\mathbf{F}}_p\mathbf{F}_p^{-1} \tag{3}$$

$$\mathbf{C}_e = \mathbf{F}_e^T\mathbf{F}_e = \mathbf{F}_p^{-T}\mathbf{C}\mathbf{F}_p^{-1} \tag{4}$$

Moreover, following from (Fereidoonnezhad et al., 2021) a further multiplicative decomposition of the elastic deformation gradient $\mathbf{F}_e = J_e^{1/3}\bar{\mathbf{F}}_e$ is considered, where J_e is the elastic volume ratio and $\bar{\mathbf{F}}_e$ is the modified isochoric elastic deformation gradient. The isochoric right Cauchy–Green elastic tensor is given as $\bar{\mathbf{C}}_e = \bar{\mathbf{F}}_e^T\bar{\mathbf{F}}_e$. The principal stretches (λ_i), modified principal stretches ($\bar{\lambda}_i$), elastic principal stretches (λ_{ie}), and isochoric elastic principal stretches ($\bar{\lambda}_{ie}$) are principal values of $\mathbf{F}$, $\bar{\mathbf{F}}$, $\mathbf{F}_e$, and $\bar{\mathbf{F}}_e$, respectively.

In (Fereidoonnezhad et al., 2021, 2020a) we propose a framework for the elastic deformation and rotation of the fibrin network in the development of anisotropic hyperelastic behaviour of blood clots. In the current study we extend this framework to incorporate the permanent plastic deformation of clots due to formation and dissociation of cross-links in the fibrin network. Considering a fibrin fibre characterised by a direction vector $\mathbf{a}_{0i}$, we define a structural tensor $\mathbf{A}_{0i}$ as

$$\mathbf{A}_{0i} = \mathbf{a}_{0i} \otimes \mathbf{a}_{0i} \tag{5}$$

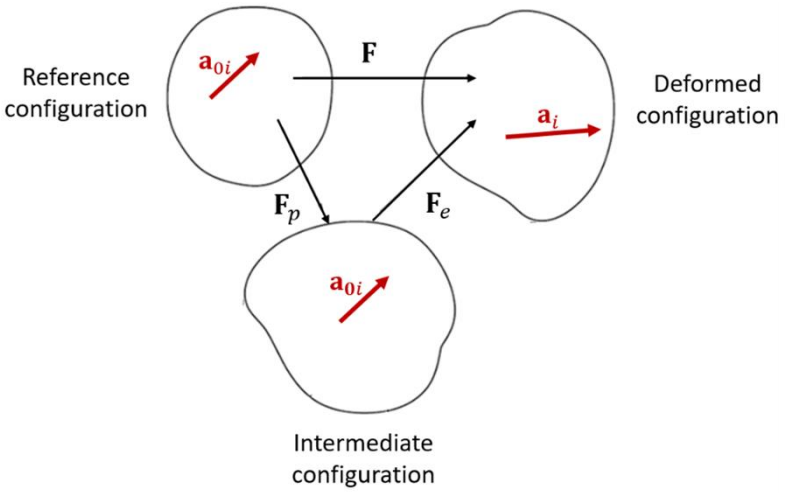

Figure 1: Schematic representation of the multiplicative decomposition of the deformation gradient tensor $\mathbf{F}$ into the plastic part $\mathbf{F}_p$ and elastic part $\mathbf{F}_e$.

An schematic representation of the multiplicative decomposition of deformation gradient $\mathbf{F}$ is shown in Figure 1. Here, we assume that the rotation is lumped into the elastic part of the deformation gradient, such that a typical fibre direction $\mathbf{a}_{0i}$ remains unrotated in the intermediate configuration and then rotate to $\mathbf{a}_i$ direction through the elastic deformation $\mathbf{F}_e$.

2.2 *Free energy and thermodynamic consistency*

The Clausius–Duhem inequality for a system with constant mass and an isothermal process is given as

$$\frac{1}{2}\mathbf{S}:\dot{\mathbf{C}} - \dot{\psi} \geq 0 \tag{6}$$

where $\mathbf{S}$ is the second Piola-Kirchhoff stress tensor, ψ is the free energy per unit volume and the first derivative of ψ with respect to time is denoted by $\dot{\psi}$.

Inequality (6) is quite general and does not include any indication of the variables upon which ψ depends. In order to obtain an explicit constitutive law, we need to specify such variables. We propose the following form of the free energy per unit volume of the tissue

$$\psi = \psi\left(\mathbf{C}_e, \mathbf{A}_{0i}\right) \tag{7}$$

The time derivative of the free energy is then calculated as:

$$\dot{\psi} = \frac{\partial \psi}{\partial \mathbf{C}_e} : \frac{\partial \mathbf{C}_e}{\partial \mathbf{C}} : \dot{\mathbf{C}} + \frac{\partial \psi}{\partial \mathbf{C}_e} : \frac{\partial \mathbf{C}_e}{\partial \mathbf{F}_p} : \dot{\mathbf{F}}_p + \frac{\partial \psi}{\partial \mathbf{A}_{0,i}} : \dot{\mathbf{A}}_{0i} \tag{8}$$

The structural tensors $\mathbf{A}_{0i}$ change only through $\mathbf{F}_e$ and $\mathbf{F}_p$, and no additional evolution law is required for fibre reorientation, such that $\dot{\mathbf{A}}_{0i} = \mathbf{0}$.

Substituting (8) into (6) then results in

$$\left(\frac{1}{2}\mathbf{S}-\frac{\partial\psi}{\partial\mathbf{C}_e}:\frac{\partial\mathbf{C}_e}{\partial\mathbf{C}}\right):\dot{\mathbf{C}}-\frac{\partial\psi}{\partial\mathbf{C}_e}:\frac{\partial\mathbf{C}_e}{\partial\mathbf{F}_p}:\dot{\mathbf{F}}_p\geq 0 \tag{9}$$

Thus, with the standard arguments of continuum thermodynamics we obtain the following expression for the second Piola–Kirchhoff stress tensor, i.e.

$$\mathbf{S}=\frac{\partial\psi}{\partial\mathbf{C}_e}:\frac{\partial\mathbf{C}_e}{\partial\mathbf{C}} \tag{10}$$

The dissipation inequality (9) then reduced to

$$-\frac{\partial\psi}{\partial\mathbf{C}_e}:\frac{\partial\mathbf{C}_e}{\partial\mathbf{F}_p}:\dot{\mathbf{F}}_p\geq 0 \tag{11}$$

After some mathematical elaboration (Fereidoonnezhad et al., 2017) equation (11) is re-written as

$$\mathbf{M}_e:\mathbf{L}_p\geq 0, \tag{12}$$

in which $\mathbf{M}_e$ is the elastic Mandel stress defined as,

$$\mathbf{M}_e=2\mathbf{C}_e:\frac{\partial\psi}{\partial\mathbf{C}_e}, \tag{13}$$

2.3 *Evolution law for plastic deformation*

We assume that the permanent deformation in blood clots, as a fibrous material, arise from cross-link formation/dissociation between the fibrin fibres. Deformation of the clot cause some fibres to come into contact and form new cross-links at the points of interactions, but also cause in dissociation of some available cross-links. As schematically demonstrated in Figure 2, we consider both isochoric and volumetric plasticity in the fibrin network. The undeformed fibrin network (Figure 2A) deformed by an isochoric shear deformation (Figure 2B) leads to dissociation of some bonds and formation of some new bonds. The formation of new cross links in the fibrin network depends on the reduction of the distance between fibres, which can be related to the minimum isochoric principal stretch $\bar{\lambda}_{min}$. The possibility of cross-link formation is higher in compact fibre network compared to a spare network. On the other hand, cross-link dissociation depends on the maximum stretch in the fibrin network, $\bar{\lambda}_{max}$. In addition, as shown in Figure 2C, D, pure volumetric deformation can also cause fibrin networks compaction ($J<1$) or expansion ($J>1$) which results in cross-links formation/dissociation and consequently induces unrecoverable plastic deformation in the fibrin network.

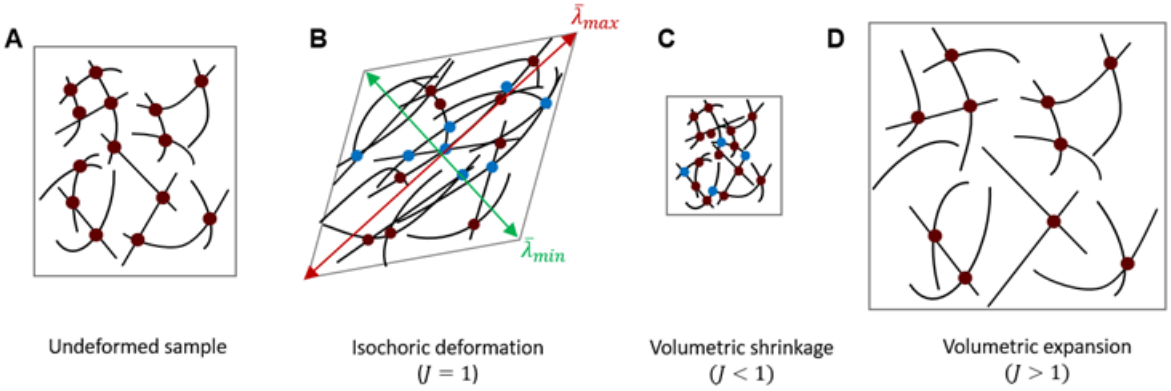

Figure 2: Schematic representation of the underlying mechanism for the unrecoverable (permanent deformation) in blood clot. (A) undeformed fibrin network with cross-links between fibres, (B) In an isochoric shear deformation, some cross-links are dissociated as a result of seperation in the principal direction with maximum stretch ($\bar{\lambda}_{max}$) and some new cross-links are formed (blue dots) as the fibrin network are compacted in the principal direction corresponding to the minimum stretch ($\bar{\lambda}_{min}$), (C) volumetrick compaction of fibrin network leads to formation of new bonds, and (D) volumetric expansion of the network cause cross-link dissociation.

These changes in the microstructure of blood clot form a new fibrin network with different constraints and deformability. This new network of fibres is not able to fully recover its original shape after removal of the applied load. We propose the following evolution law for the density of cross-links in the fibrin network:

$$\dot{\rho}_c = k_1 \exp\left(\frac{1-\bar{\lambda}_{min}}{a_1}\right) H\left(1-\bar{\lambda}_{min}\right) - k_2 \exp\left(\frac{\bar{\lambda}_{max}-1}{a_2}\right) \rho_c H\left(\bar{\lambda}_{max}-1\right) + k_3 (J-1)^{2n_1} H(1-J) - k_4 (J-1)^{2n_1} \rho_c H(J-1) \tag{14}$$

where $H(\mathrm{x})$ denotes the unit step function and $k_1, k_2, k_3, k_4, a_1, a_2$ and n_1 are material parameters. The first two terms in equation (14) represent the changes in the density of cross-links due to the isochoric deformation where the first term specify the formation of new cross-links and the second term represents the dissociation of cross-links. The third and fourth terms of equation (14) incorporate the influence of volume changes (compaction/expansion of the fibrin network) on the formation and dissociation of cross links, respectively.

Moreover, we propose the following form for the plastic deformation gradient tensor $\mathbf{F}_p$

$$\mathbf{F}_p = \theta_p \mathbf{I} + \left(\lambda_p - \theta_p\right) \mathbf{n} \otimes \mathbf{n} \tag{15}$$

where $\mathbf{n}$ is the principal direction corresponding to the maximum principal stretch, and λ_p, θ_p are plastic stretches in the principal direction $\mathbf{n}$ and transverse to the direction $\mathbf{n}$, respectively. The plastic velocity gradient $\mathbf{L}_p$ is then calculated as

$$\mathbf{L}_p = \frac{\dot{\theta}_p}{\theta_p} \mathbf{I} + \left(\frac{\dot{\lambda}_p}{\lambda_p} - \frac{\dot{\theta}_p}{\theta_p}\right) \mathbf{n} \otimes \mathbf{n} \tag{16}$$

We further propose the following relationship between the plastic stretches

$$\theta_p = \lambda_p^{-\nu} \tag{17}$$

Substituting equations (16) and (17) into inequality (12) results in:

$$\frac{\dot{\lambda}_p}{\lambda_p} \mathrm{X} \geq 0, \quad \mathrm{X} = -\nu \mathrm{tr}(\mathbf{M}_e) + (1+\nu)\mathrm{tr}(\mathbf{M}_e : \mathbf{N}) \tag{18}$$

Permanent deformation is an irreversible dissipative process and $\dot{\lambda}_p$ is always non-negative. Therefore, the necessary conditions for $\dot{\lambda}_p$ to satisfy the second law of thermodynamics (equation (12)) are (Ebrahimi et al., 2021):

$$\begin{cases} \dot{\lambda}_p > 0, & \mathrm{X} \geq 0 \\ \dot{\lambda}_p = 0, & \mathrm{X} < 0 \end{cases} \tag{19}$$

Considering the constraint (19) and note that λ_p is the plastic stretch due to the cross-link formation/dissociation we propose the following evolution law

$$\dot{\lambda}_p = |\dot{\rho}_c| \langle \lambda_{max} - \lambda_p \rangle^m H(\mathrm{X}) \tag{20}$$

where $\langle x \rangle$ and $H(\mathrm{x})$ denote McCauley bracket and unit step function, respectively, λ_{max} is the maximum principal stretch, and $\dot{\rho}_c$ is time variation of the density of cross-links in the fibrin network.

2.4 *Specific form of free energy*

The general form of free energy in equation (7) is additively decomposed as

$$\psi\left(\mathbf{C}_e, \mathbf{A}_0^i\right) = \psi_{vol}\left(J_e\right) + \psi_{iso}\left(\bar{\lambda}_{1e}, \bar{\lambda}_{2e}, \bar{\lambda}_{3e}\right) + \sum_{i=1}^{N} \psi_{f,i}\left(\lambda_{fe,i}\right) \tag{21}$$

where, ψ_{vol} is the volumetric strain energy, ψ_{iso} is the isochoric strain energy corresponding to the non-fibrous matrix, $\bar{\lambda}_{ie}$ $(i = 1,2,3)$ are the principal values of $\bar{\mathbf{C}}_e$, and J_e=$\lambda_{1e}\lambda_{2e}\lambda_{3e}$ is the elastic jacobian. In addition, $\psi_{f,i}$ $(i = 1, \dots, N)$ are the contribution of fibrin fibres in free energy, and $\lambda_{fe,i} = \sqrt{\mathbf{a}_{0i} . \mathbf{C}_e \mathbf{a}_{0i}}$ $(i = 1, \dots, N)$ are elastic fibre stretches. We then employ the following models for each part of the strain energy as proposed in our previous works (Fereidoonnezhad et al., 2021, 2020b):

$$\psi_{iso}\left(\bar{\lambda}_{1e}, \bar{\lambda}_{2e}, \bar{\lambda}_{3e}\right) = \sum_{i=1}^{3} \bar{\psi}\left(\bar{\lambda}_{ie}\right), \tag{22}$$

$$\bar{\psi}(\bar{\lambda}_{ie}) = \begin{cases} E_{1\mathrm{m}}(\bar{\lambda}_{ie} - \ln\bar{\lambda}_{ie} - 1) & |\bar{\lambda}_{ie} - 1| \le D_{1m} \\ p_m\left(\frac{\bar{\lambda}_{ie}{}^2}{2} - 2\bar{\lambda}_{ie} + \ln\bar{\lambda}_{ie}\right) + q_m(\bar{\lambda}_{ie} - \ln\bar{\lambda}_{ie}) + r_m\ln\bar{\lambda}_{ie} + \psi_{01m} & D_{1m} < |\bar{\lambda}_{ie} - 1| < D_{2m} \\ E_{2m}(\bar{\lambda}_{ie} - (1 + D_{2m})\ln\bar{\lambda}_{ie}) + (p_m D_{2m}^2 + q_m D_{2m} + r_m)\ln\bar{\lambda}_{ie} + \psi_{02m} & |\bar{\lambda}_{ie} - 1| \ge D_{2m} \end{cases}$$

where $D_{1m}, D_{2m}, E_{1m},$ and E_{2m} are material parameters, and ψ_{01m} and ψ_{02m} are two constants which ensure the continuity of strain energy. Moreover $p_m, q_m,$ and r_m are not independent parameters; in order to maintain C^0 and C^1 continuity the following relations must be enforced:

$$p_m = \frac{E_{1m} - E_{2m}}{2(D_{1m} - D_{2m})}, \quad q_m = E_{1m} - 2D_{1m}p_m, \quad r_m = (E_{1m} - q_m)D_{1m} - p_m D_{1m}^2 \tag{23}$$

The non-linear volumetric behaviour of clot is also represented as

$$\psi_{vol}(J) = \begin{cases} \kappa_1(J - \ln J_e - 1) & |J_e - 1| \le D_{1v} \\ p_v\left(\frac{J_e{}^2}{2} - 2J_e + \ln J_e\right) + q_v(J_e - \ln J_e) + r_v\ln J_e + \psi_{01v} & D_{1v} < |J_e - 1| < D_{2v} \\ \kappa_2(J_e - (1 + D_{2v})\ln J_e) + (p_v D_{2v}^2 + q_v D_{2v} + r_v)\ln J_e + \psi_{02v} & |J_e - 1| \ge D_{2v} \end{cases} \tag{24}$$

in which κ_1 and κ_2 are the initial small-strain and large-strain bulk modulus, respectively, the parameters D_{1v} and D_{2v} control the transition volumetric strains, and $p_v, q_v,$ and r_v are obtained in a similar manner as equation (23) by using the corresponding volumetric parameters. The strain energy density function for fibrin fibres is also represented as (Fereidoonnezhad et al., 2020b)

$$\psi_{f,i} = \begin{cases} E_{1f}\left(\frac{2}{3}\lambda_{fe,i}^3 - \lambda_{fi}^2 + \frac{1}{3}\right), & \lambda_{fi} - 1 \le D_{1f} \\ \frac{2}{3}\lambda_{fe,i}^3(q_f - 2p_f) + \frac{p_f}{2}\lambda_{fe,i}^4 + \lambda_{fe,i}^2(p_f - q_f + r_f) + \psi_{01f}, & D_{1f} < \lambda_{fi} - 1 < D_{2f} \\ \frac{2E_{2f}}{3}\lambda_{fe,i}^3 + \lambda_{fe,i}^2(p_f D_{2f}^2 + q_f D_{2f} + r_f - E_{2f} - E_{2f}D_{2f}) + \psi_{02f}, & \lambda_{fi} - 1 \ge D_{2f} \end{cases} \tag{25}$$

where D_{1f} and D_{2f} are transition strains of the fibres, E_{1f} and E_{2f} are material parameters, ψ_{01f} and ψ_{02f} are two constants which ensure the continuity of strain energy and $p_f, q_f,$ and r_f are obtained in a similar manner as equation (23) by using the corresponding parameters for fibres.

2.5 *Numerical implementation*

To solve the governing equations numerically, we implement the proposed constitutive equations into the FE framework via the user subroutine material UMAT in Abaqus ("Abaqus 2017. Analysis User's Guide, Dassault Systèmes Simulia Corp.," 2017). In the following we describe how the stress is calculated.

Given the deformation gradient tensor $\mathbf{F}$, $\bar{\lambda}_{max}$, $\bar{\lambda}_{min}$, and J are calculated and then an implicit backward-Euler time integration scheme is employed to calculate the incremental update of the density of cross-link, ρ_c, from equation (14) as

$$\rho_c^{n+1} = \frac{\rho_c^n + k_1 \exp\left(\frac{1-\bar{\lambda}_{min}}{a_1}\right) H\left(1-\bar{\lambda}_{min}\right)\Delta t + k_3 (J-1)^{2n_1} H(1-J)\Delta t}{1 + k_2 \exp\left(\frac{\bar{\lambda}_{max}-1}{a_2}\right) H\left(\bar{\lambda}_{max}-1\right)\Delta t + k_4 (J-1)^{2n_1}\Delta t H(J-1)\Delta t} \tag{26}$$

where the superscripts n and $n+1$ stands for the value of the parameter at time t_n and $t_{n+1} = t_n + \Delta t$, respectively. We also use the backward-Euler time integration scheme to discretise the evolution equation of plastic stretch λ_p (equation (20)) as

$$\frac{\lambda_p^{n+1} - \lambda_p^n}{\Delta t} = \frac{|\rho_c^{n+1} - \rho_c^n|}{\Delta t} \langle \lambda_{max} - \lambda_p^{n+1} \rangle^m H(\mathrm{X}) \tag{27}$$

It is noted that we have already calculated ρ_c^{n+1} from (26) and the only unknown of equation (27) is λ_p^{n+1}. However, since equation (27) is nonlinear it is not possible to find a close form solution for λ_p^{n+1}. Therefore, an iterative Newton-Raphson method is employed to solve equation (27). The plastic stretch θ_p is then calculated from equation (17) and consequently the plastic deformation gradient $\mathbf{F}_p$ and the elastic deformation gradient $\mathbf{F}_e$ are calculated from (15) and (1), respectively. Having $\mathbf{F}_e$, the stress tensor is then calculated from (10), as explained in our previous paper (Fereidoonnezhad et al., 2020b).

3. Numerical Examples

3.1 *Material parameters identification*

In Figure 3A we demonstrate that the proposed material formulation accurately reproduces experimentally observed nominal stress-strain behaviour of whole blood clot subjected to load-unload uniaxial tension with strain rate of 0.1 sec^{-1} (Sugerman et al., 2020). The nonlinear least-square method in Matlab has been used to calibrate the model to the experimental data and the optimised parameters are provided in Table 1. In section 3.3, we use the calibrated parameters to highlight the importance of considering the permanent deformation of clot in predicting the outcomes of aspiration thrombectomy. The computed evolution of the plastic stretch (λ_p) for the whole blood clot subjected to load-unload uniaxial tension is shown in Figure 3B.

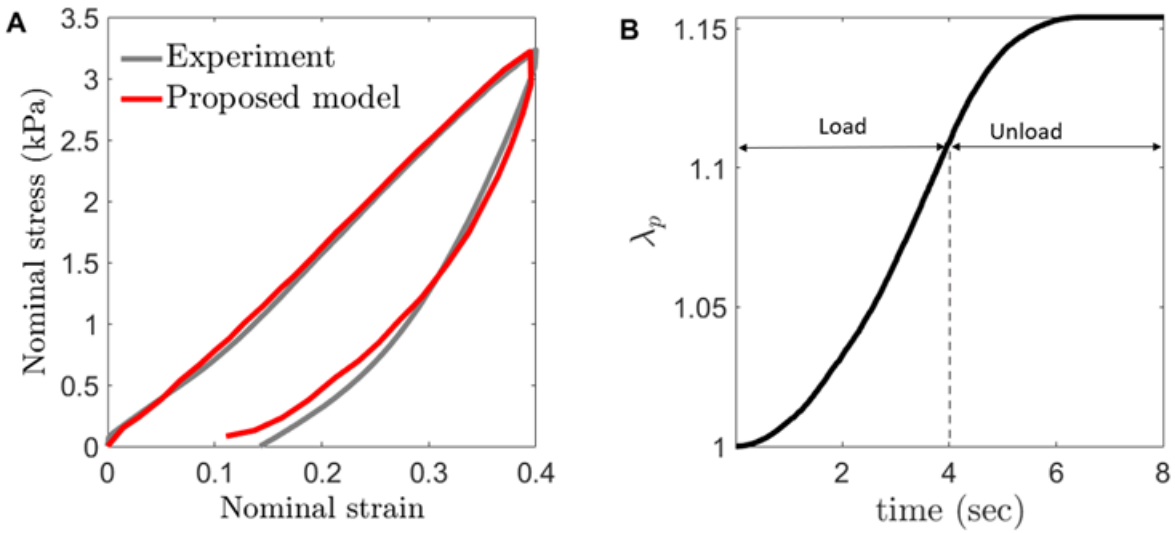

Figure 3: (A) Capability of the proposed model to replicate the experimental data of load-unload uniaxial tension test for whole blood clot (Sugerman et al., 2020), (B) Evolution of the plastic stretch λ_p during load-unload uniaxial tension test.

Table 1: Calibrated material parameters of the proposed plastic model and the purely hyperelastic model for whole blood clot (Sugerman et al., 2020).

Parameter	Proposed plastic model	Hyperelastic model
$D_{1m}\,(-)$	0.1	0.2
$D_{2m}\,(-)$	0.2	0.6
$E_{1m}(\mathrm{kPa})$	3	4
$E_{2m}(\mathrm{kPa})$	8	9
$D_{1f}\,(-)$	0.05	0.2
$D_{2f}\,(-)$	0.1	0.4
$E_{1f}(\mathrm{kPa})$	9	8
$E_{2f}(\mathrm{kPa})$	25	20
$D_{1v}\,(-)$	0.01	0.01
$D_{2v}\,(-)$	0.05	0.05
$\kappa_1(\mathrm{kPa})$	30	30
$\kappa_1(\mathrm{kPa})$	80	80
$k_1\,(\mathrm{sec}^{-1})$	0.25	–
$k_2\,(\mathrm{sec}^{-1})$	0.1	–
$k_3\,(\mathrm{sec}^{-1})$	8.5	–
$k_4\,(\mathrm{sec}^{-1})$	0.8	–
$a_1\,(-)$	0.5	–
$a_2\,(-)$	1	–
$n_1\,(-)$	2	–
$m\,(-)$	1	–
$v\,(-)$	0.5	–

3.2 *Sensitivity analysis of the model*

To demonstrate the main features of the developed model, a parameter sensitivity study is presented in Figure 4 where the clot is subjected to uniaxial loading-unloading boundary conditions described in Section 3.1. The calibrated material parameters for the whole blood clot (Table 1) have been used as the baseline parameters. Figure 4 demonstrates that, for the given material parameters, k_1, k_2, a_1, a_2, and m have significant influence on the stress-strain results in uniaxial tension test. These parameters associated with the role of isochoric deformation on the permanent deformation. On the other hand, parameters k_3, k_4, and n_1, which represent the role of volumetric deformation on the induced plasticity, do not significantly influence the response to applied uniaxial tension. Future experimental studies should investigate the permanent deformation of thrombus due to volumetric compaction/expansion.

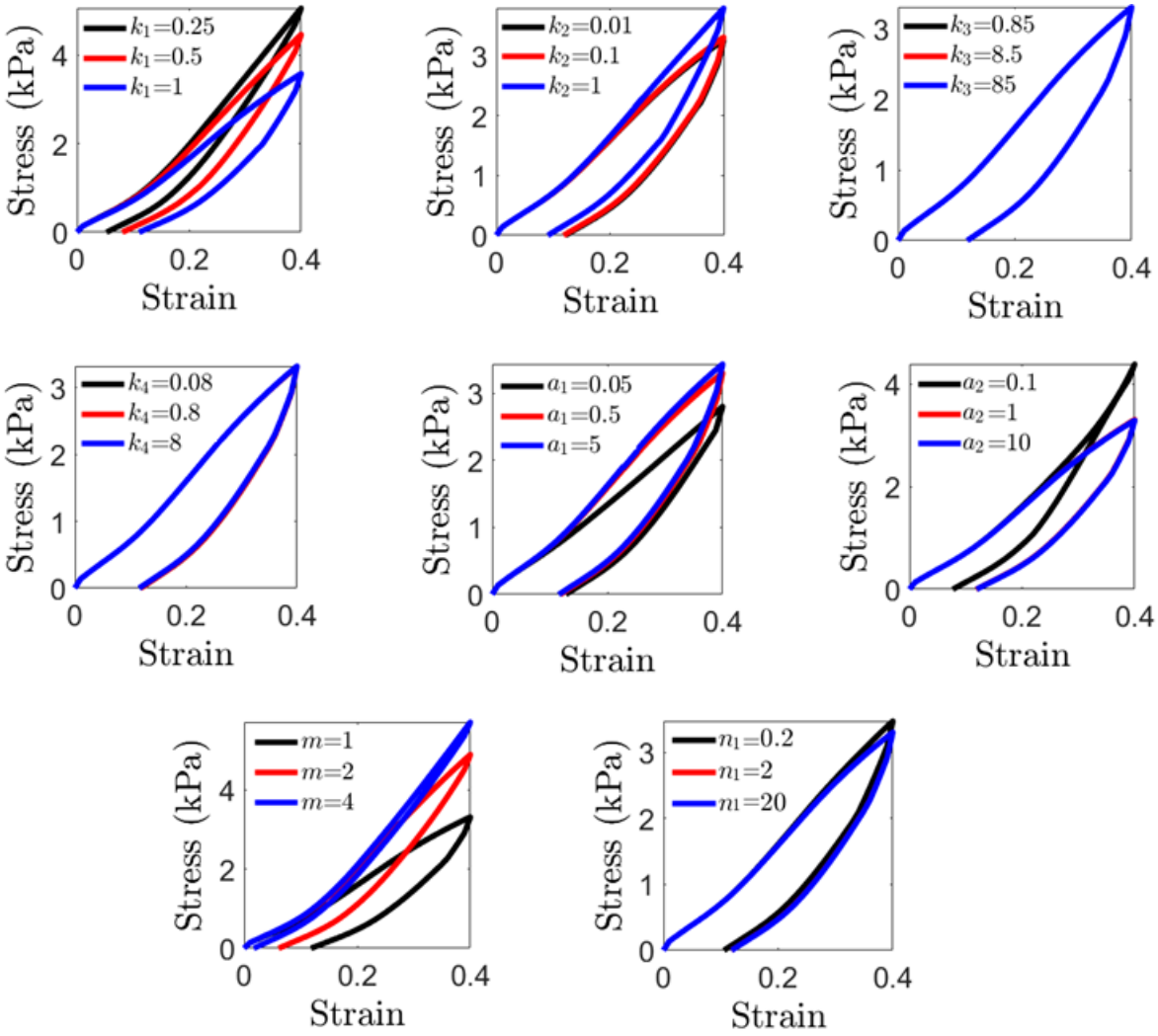

Figure 4: Sensitivity analysis of the proposed model in terms of the parameters corresponding to permanent defrmation in load-unload uniaxial tension test. The nominal stress vs. nominal strain is shown and the material parameters in Table 1 have been used as baseline parameters in all figures.

3.3 *Simulation of Aspiration thrombectomy*

Model construction: The objective of this section is to demonstrate the influence of plastic (permanent) deformation on aspiration thrombectomy by performing finite element simulations of the interaction between a clot and an aspiration catheter (Figure 5A). Three aspiration catheter designs with diameters of 1.5 mm, 1.8 mm, 2 mm are considered, with a cylindrical clot of 3 mm diameter and 10 mm length. A suction pressure, linearly increasing from 0 mmHg to 200 mmHg over 5 seconds, is applied to the portion of the clot which is inside the catheter. The developed constitutive model, with the calibrated material parameters in Table 1, has been used to model the blood clot and the catheter is assumed as a rigid body. The aspiration length, *u*, is defined as the distance that the top surface of the clot moves into the catheter. In order to demonstrate the contribution of plasticity to clot deformation, simulations are also performed for a purely hyperelastic clot (equations (21)-(25)) in which material properties (Table 1) are calibrated to reproduce the loading curve in Figure 3A. A mesh sensitivity study reveals that a converged solution is obtained using 24000 axisymmetric quadrilateral elements of type CAX4.

Results: The computed aspiration length, *u*, for three catheter diameters is shown in Figure 4B, both for the proposed plasticity clot model and the purely hyperplastic clot model. As expected, an increase in catheter diameter results in an increase in aspiration length, *u*. Importantly, simulations suggest that permanent plastic deformation results in a 10-15% increase in aspiration length at an applied pressure of 200 mmHg. In other words, if plasticity is omitted from the model the aspiration length is significantly under-predicted.(Figure 5B).

Distribution of the maximum principal stress in clot at the point of maximum applied pressure for all three catheter sizes, predicted by the proposed plastic model, and by the purely hyperelastic model, are shown in Figure 5C. The results suggest that the hyperelastic model overpredicts the maximum stress in the clot by 10-13%. The computed values of maximum principal stress for both models are lower than the critical values of crack initiation for different clot compositions (100-480 kPa), as reported in our previous study (Fereidoonnezhad et al., 2020a).

Finally, the computed distributions of unrecoverable plastic stretch (λ_p) in the clot for all three catheter sizes are shown in Figure 5D. Very high plastic strains (~20 %) are computed near the opening of the aspiration catheter, highlighting the significant level of induced permanent deformation during aspiration.

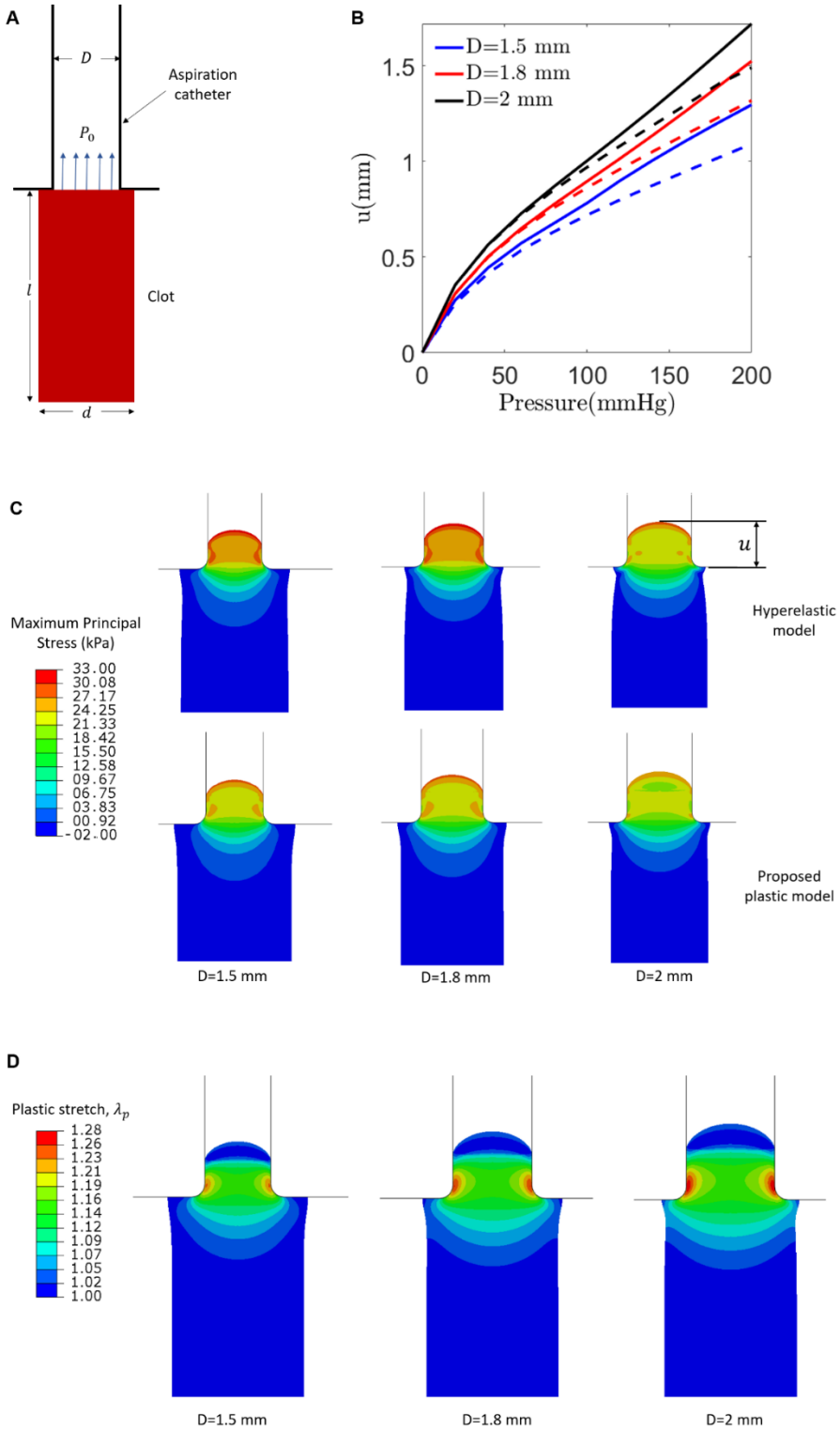

Figure 5: Finite element simulation of clot removal in aspiration thrombectomy. (A) Three catheters with bore diameters of $D = 1.5\ mm, 1.8\ mm, 2\ mm$ are used for the aspiration of a cylindrical clot with length of $l = 10\ mm$ and diameter of $d = 3\ mm$, and a suction pressure, linearly increasing from 0 mmHg to 200 mmHg over 5 seconds, is applied to the portion of the clot which is inside the catheter, (B) Centre point displacement of clot (u) for three catheter sizes in the cases of hyperelastic model and the proposed model with permanent deformation, (C) Distribution of the maximum principal stress (MPa) in clot at the point of maximum applied pressure for the hyperelastic model and the proposed plastic model, and (D) the calculated distribution of unrecoverable plastic stretch (λ_p) in the clot for all catheter sizes.

4. Conclusions

In this study we have proposed a new material model for the permanent plastic deformation of thrombus material. This new formulation is incorporated into our recently developed anisotropic hyperelastic model that describes elastic deformation and rotation of the fibrin network. The model is developed based on the deformation-induced microstructural changes in fibrin network, including the formation and dissociation of the cross-links between fibrin fibres. We demonstrate that the addition of our new plasticity formulation allows for the accurate simulation of recent experiment measurements of permanent thrombus deformation following uniaxial stretching (Sugerman et al., 2020). We then present simulations of aspiration of a clot into a catheter, demonstrating the importance of our plasticity mechanism in the deformation of the clot. This model provides a basis for design and assessment of novel aspiration catheter design to improve the first-pass revascularization rate in aspiration thrombectomy.

Future work should investigate the influence of catheter design and loading profile (e.g. cyclic versus static pressure) on the performance of aspiration thrombectomy of a clot, incorporating the plastic and hyperelastic mechanisms developed in the current study. Large-bore aspiration catheters demonstrate improved recanalization rates compared to smaller lumen devices in aspiration thrombectomy (Long et al., 2019). On the other hand, smaller catheters have the advantage of better navigability and allow easier access to the occlusion site. The current study suggests that higher levels of plastic deformation will occur for small diameter catheters. The future works should also consider the risk of clot fragmentation while it is sucked into the aspiration catheter as it may result in distal embolization.

Future experimental data are required to calibrate/validate the developed model for volumetric plasticity during compaction, and permanent fibre alignment due to the plastic deformation of thrombus. Influence of clot composition (fibrin content) on permanent deformation and influence of plasticity on fracture resistance of thrombus should also be investigated in future studies.

5. Acknowledgment

This work has received funding from the European Union’s Horizon 2020 research and innovation programme under grant agreement No 777072.

6. References

Abaqus 2017. Analysis User's Guide, Dassault Systèmes Simulia Corp., 2017.

Chueh, J.Y., Wakhloo, A.K., Hendricks, G.H., Silva, C.F., Weaver, J.P., Gounis, M.J., 2011. Mechanical characterization of thromboemboli in acute ischemic stroke and laboratory embolus analogs. Am. J. Neuroradiol. 32, 1237–1244. https://doi.org/10.3174/ajnr.A2485

Ebrahimi, P., Arghavani, J., Sohrabpour, S., McGarry, P., Naghdabadi, R., 2021. Microstructure-based finite deformation modelling of super-elastic NiTi shape memory alloy considering various inelastic mechanisms. Prepr.

Fereidoonnezhad, B., Dwivedi, A., Johnson, S., McCarthy, R., McGarry, P., 2020a. Blood clot fracture properties are dependent on red blood cell and fibrin content. Acta Biomater. (under Rev.

Fereidoonnezhad, B., Moerman, K.M., Johnson, S., McCarthy, R., Mcgarry, P.J., 2021. A new compressible hyperelastic model for the multi-axial deformation of blood clots occlusion in vessels. https://doi.org/10.31224/osf.io/jdngb.

Fereidoonnezhad, B., Naghdabadi, R., Sohrabpour, S., Holzapfel, G.A., 2017. A Mechanobiological model for damage-induced growth in arterial tissue with application to in-stent restenosis. J. Mech. Phys. Solids 101. https://doi.org/10.1016/j.jmps.2017.01.016

Fereidoonnezhad, B., O'Connor, C., McGarry, P., 2020b. A new anisotropic soft tissue model for elimination of unphysical auxetic behaviour. J. Biomech. 111, 110006. https://doi.org/10.1016/j.jbiomech.2020.110006

Gralla, J., Schroth, G., Remonda, L., Nedeltchev, K., Slotboom, J., Brekenfeld, C., 2006. Mechanical thrombectomy for acute ischemic stroke: Thrombus-device interaction, efficiency, and complications in vivo. Stroke 37, 3019–3024. https://doi.org/10.1161/01.STR.0000248457.55493.85

Johnson, S., Chueh, J., Gounis, M.J., McCarthy, R., McGarry, J.P., McHugh, P.E., Gilvarry, M., 2019. Mechanical behavior of in vitro blood clots and the implications for acute ischemic stroke treatment. J. Neurointerv. Surg. 1–6. https://doi.org/10.1136/neurintsurg-2019-015489

Johnson, S., Ray McCarthy, Peter McHugh, Mcgarry, P., McCarthy, R., Gilvarry, M., McHugh, P.E., McGarry, J.P., 2020. Investigating the Mechanical Behaviour of Clot Analogues through Experimental and Computational Analysis. Ann. Biomed. Eng. 1–12. https://doi.org/10.1007/s10439-020-02570-5

Kaesmacher, X.J., Boeckh-Behrens, T., Simon, S., Maegerlein, C., Kleine, J.F., Zimmer, C., Schirmer, L., Poppert, H., Huber, T., 2017. Risk of thrombus fragmentation during endovascular stroke treatment. Am. J. Neuroradiol. 38, 991–998. https://doi.org/10.3174/ajnr.A5105

Kowoll, A., Weber, A., Mpotsaris, A., Behme, D., Weber, W., 2016. Direct aspiration first pass technique for the treatment of acute ischemic stroke: Initial experience at a European stroke center. J. Neurointerv. Surg. 8, 230–234. https://doi.org/10.1136/neurintsurg-2014-011520

Long, T.D., Kallmes, D.F., Hanel, R., Shigematsu, T., Halaszyn, A.M., Wolter, J., Berenstein, A., 2019. Novel aspiration catheter design for acute stroke thrombectomy. J. Neurointerv. Surg. 11, 179–183. https://doi.org/10.1136/neurintsurg-2017-013702

Maus, V., Behme, D., Kabbasch, C., Borggrefe, J., Tsogkas, I., Nikoubashman, O.,

Wiesmann, M., Knauth, M., Mpotsaris, A., Psychogios, M.N., 2018. Maximizing First-Pass Complete Reperfusion with SAVE. Clin. Neuroradiol. 28, 327–338. https://doi.org/10.1007/s00062-017-0566-z

Po Sit, S., 2009. The penumbra pivotal stroke trial: Safety and effectiveness of a new generation of mechanical devices for clot removal in intracranial large vessel occlusive disease. Stroke 40, 2761–2768. https://doi.org/10.1161/STROKEAHA.108.544957

Sugerman, G.P., Parekh, S.H., Rausch, M.K., 2020. Toward understanding thrombus fracture: Dissipative phenomena of whole blood clots. https://doi.org/10.1101/2020.07.19.210765

WHO global health estimate [WWW Document], 2020. URL https://www.who.int/news-room/fact-sheets/detail/the-top-10-causes-of-death

Yoo, A.J., Andersson, T., 2017. Thrombectomy in acute ischemic stroke: Challenges to procedural success. J. Stroke. https://doi.org/10.5853/jos.2017.00752

Zaidat, O.O., Ribo, M., Mattle, H.P., Saver, J.L., Bozorgchami, H., Yoo, A.J., Ehm, A., Kottenmeier, E., Cameron, H.L., Qadeer, R.A., Andersson, T., 2020. Health economic impact of first-pass success among patients with acute ischemic stroke treated with mechanical thrombectomy: A United States and European perspective. J. Neurointerv. Surg. https://doi.org/10.1136/neurintsurg-2020-016930